ISTITUTO NAZIONALE DI FISICA NUCLEARE

Sezione di Torino

INFN/TC-92/10
13 Aprile 1992

M. Boero, C. Manfredotti, C. Ongaro, A. Zanini :

EVALUATION OF THE NEUTRON YIELD PRODUCED IN A D-D + D-T PLASMA BY MONTE CARLO SIMULATION

INFN – Istituto Nazionale di Fisica Nucleare
Sezione di Torino

INFN/TC–92/10
13 Aprile 1992

EVALUATION OF THE NEUTRON YIELD PRODUCED IN A D–D + D–T PLASMA BY MONTE CARLO SIMULATION

C. Manfredotti, A. Zanini *, C. Ongaro and M. Boero

Experimental Physics Dept., University of Torino and
*Istituto Nazionale di Fisica Nucleare - sezione di Torino

Abstract

The neutron yield obtained from nuclear fusion reactions represents a straightforward indication of the fusion power generated inside a plasma.

A JET–like apparatus has been reproduced and computer simulations carried out with the help of Monte Carlo Neutron Photon (MCNP) code [1] in order to test for neutron production and flux coming out from a D–D and D–T plasma.

A detection channel has been set up beside the torus chamber and the simulated neutron yield calculated in five different angular positions related to the various sections of the plasma view–angle resolved by means of a pin–hole.

In addition letargy calculations on neutron kinematics have been performed to estimate the elastic scattering processes which are responsible of appearance of neutrons with energies far from the D–D and D–T peaks detected at the bottom of the horizontal port.

1. Introduction

The neutron diagnostics provides a useful tool to obtain informations on the plasma parameters. In deuterium–deuterium (D–D) and deuterium–tritium (D–T) fusion reactions, 2.45 MeV and 14.02 MeV neutrons are respectively produced and detected in regions far from the plasma. From measurements of total yield and spectral distribution and from estimations of the peak widths it is possible to know the ion temperature inside the plasma [1, 3]. Monte Carlo simulations runs have been carried out in order to reproduce a typical experimental result in plasma diagnostics and to analyze the informations which can be obtained.
The MCNP computer simulations analyzed in the following are referred to neutron fluxes outcoming from a detection channel placed at the side of a general torus chamber containing the magnetically confined plasma.

The calculated yields on the below described simulated fusion apparatus have given a statistically consistent set of outputs and the spectra obtained in different positions have been analyzed by means of neutron kinematics.

2. Reactor structure reconstruction

A toroidal ring section has been assumed which reproduces the vacuum vessel. It is surrounded by iron represented as a greater coaxial torus and with thickness larger than the mean free path of neutrons. A smaller coaxial toroidal cell inside the mentioned chamber simulates the region occupied by the plasma itself and it is regarded as the physical volume where the source of neutrons is placed.

Then a horizontal port for plasma diagnostics has been reproduced together with the pin–hole structure set up inside in order to select the neutron fluxes coming from different parts of the plasma seen at different angles by the cells placed at the outer limit of the port.

For our purposes and in order to simplify the geometry of the problem, the sections of both the vessel and the plasma have been supposed to be ellyptical instead of the typical D–shape usually reported. This has however no influence on the quality of the results obtained [2].

The scheme relative to the geometrical structure simulated is shown in fig.1. The pin–hole device has been supposed to be iron–made according to the hypothesis adopted for the rest of the coverage of the vacuum vessel and the detection channel.

Track splitters represented by surfaces have been placed along the port in order to improve the number of events and the statistical meaning of the yields counted [1]. This is an important tool provided by the MCNP computer code which enables to reduce the true number of events originally generated into the source cell identified by the central torus inside the vessel in fig.1. This has been done in order to lower the CPU time which is one of the main difficulties to overcome.

The frame has been chosen with the x coordinate along the axis of the horizontal port so that the final cells shown in fig.1 are symmetrically displaced at different azimut angles θ_k evaluated from the x axis itself. The positions of these cells have been labelled with the angle index (see Fig.1) and the overimposed simmetry implies $\theta_{-i} = -\theta_i$

3. Neutron source details

The spectral distribution of the neutrons produced in D–D or D–T fusion reactions have typical gaussian shape [3] if the square root of the energy, instead of the energy E, is adopted as variable,

$$f(E) \sim \exp\left[-\frac{(\sqrt{E}-\sqrt{B})^2}{W^2}\right] \quad . \tag{1}$$

where B is the neutron fusion energy peak and $W = FWHM/(\log\ 16)^{1/2}$.

The ion temperature T_i is directly related to $FWHM$ by means of the well established equations

$$FWHM_{D-D} = 82 \cdot \sqrt{KT_i} \qquad FWHM_{D-T} = 177 \cdot \sqrt{KT_i} \tag{2a}$$

where K is the Boltzmann constant and the sensitivity on $FWHM$ value is consequently related to the ion temperature one by [3]

$$d(FWHM)_{D-D} = \frac{41}{\sqrt{KT_i}} K dT_i \qquad d(FWHM)_{D-T} = \frac{88.5}{\sqrt{KT_i}} K dT_i \quad . \tag{2b}$$

To get a useful normalization during the calculation, the following scaling constant has been chosen

$$f(B_{D-T}) = \max_{0<E<15\ MeV}\{f(E)\} \quad ,$$

which represent the absolute maximum of the global distribution D–D + D–T, so the correctly normalized form of (1) becomes

$$f(E) = \frac{1}{\max\{f(E)\}} \exp\left[-\frac{(\sqrt{E}-\sqrt{B})^2}{W^2}\right] \quad , \tag{3}$$

while the global distribution of the source can be written as

$$f_{tot}(E) = f_{D-D}(E) + f_{D-T}(E)$$

due to the fact that the two peaks are well separate on the energy axis and their shapes are very narrow, so that the overlap is negligible [4].

The input values of fusion energies B of the two reaction and of the relative $FWHM$s are

$$B_{D-D} \simeq 2.4750\ MeV \qquad B_{D-T} \simeq 14.076\ MeV$$

$$FWHM_{D-D} \simeq 0.2657\ MeV \qquad FWHM_{D-T} \simeq 0.5623\ MeV \quad .$$

As we are interested only in neutrons coming out from the detection port, a forward emission probability from the source has been imposed, giving a statistical weight to the emission angle

$$P(\cos\varphi) = e^{\cos\varphi} \tag{4}$$

where, once again, φ is measured from the x axis of the laboratory frame. This has been done in order to partially avoid lack of events evolving in undesired directions, useless with

4. Results about MCNP and discussion

The MCNP code adopted provides an output function $Y(E_m, \theta_k)$ which gives the neutron yield, averaged over the transit time inside the cell, as a function of both detection angle and energy. The energy range has been divided into intervals ΔE_m $(m = 1, ..., N)$ and each of them represent a bin where a neutron history can terminate. The results presented as histograms are then identified by the following expression

$$Y(E_m, \theta_k) = \int_{\Delta t} \int_{\Delta E_m} \Phi(\vec{r}, E, t)\; dE\; dt \quad , \tag{5}$$

where E_m is the mesh point of ΔE_m and

$$\Phi(\vec{r}, E, t) = |\vec{v}|\; n(\vec{r}, E, t) \quad , \tag{6}$$

being $\vec{v}$ the average velocity of the particle crossing the cell and whose modulus can be deduced from the kinetic energy E_{kin}, $v = \sqrt{2E_{kin}/m_n}$. Furthermore, $n(\vec{r}, E, t)$ is the generalized particle density, i.e. their total statistical weight divided by the cell volume.

As it can be easily remarked from Fig.1, the radial positions of the cells can be considered as a constant as their distances from the plasma r_k is much greater than the distance among them, i.e. $\forall\, k' \neq k$ it is always true that $|r_k - r_{k'}|/r_k \ll 1$. The index k is the afore defined cell label.

On each angular position θ_k the neutron yields have been plotted as histograms, so a discrete angular resolution of the neutron flux can be gained and different regions of the plasma scanned.

It is quite evident that the thermalization of neutrons to low energies, i.e.energies below $\sim 2.5\; eV$, gives rise to a sort of mask effect of the D–D peak which apparently disappears, also due to the natural attenuation of the flux far from the source [5, 6]. As a matter of fact, the neutron flux linear attenuation coefficient has been evaluated as

$$-\frac{1}{\Phi}\frac{d\Phi}{dx} = \mu = 7.01 \cdot 10^{-3} cm^{-1} \quad .$$

The higher the angle θ_k the stronger the masking. The reason is the vicinity of the pin–hole walls which are responsible of low–angle elastic scattering of the neutrons that arrive at the cell. Such an effect emphasizes going nearer to the pin–hole surfaces, while it is sensitively reduced in the central detection cell. Despite this the unmasking of the D–D peak is not complete, and a residual peak can only be guessed [7] .

The main tool is the possibility of observation of different sections of the plasma region as the view angle is selected by the pin–hole, which, then, allows a kind of space–resolved diagnosis [6].

At large angles $(\theta_2,\ ,\theta_{-2})$ the whole spectrum is remarkably reduced up to 2 orders of magnitude due to the fact that thinner sections of the plasma torus are seen with respect to the central angle θ_0 and because of the choice of the initial direction of the particles forced to be preferentially forward oriented as quoted before. Neutron yields histograms are shown in Figg.2 a–e.

In spite of the fact that the D–D peak vanishes, it is possible to estimate its $FWHM$ by means of a fit with an overposition of a gaussian–like function and an exponential one in the region below $\sim 5\ eV$. The choice of the gaussian–like function is suggested by the source distribution (1). A similar analysis can be performed also on the D–T and a significative example about the results of this kind of calculations is shown in fig.3 for the central detection cell. It is possible to carry out this fitting procedure also on the remaining cells, but no appreciable changes in $FWHM$s have been shown. Only the amplitude of the gaussian–like distribution functions reduces.

A decreasing in the $FWHM$s values with respect to the source ones has suggested to set up two empirical scaling factors

$$\beta_{D-D} = \frac{FWHM^{source}_{D-D}}{FWHM^{yield}_{D-D}} = 1.77$$

$$\beta_{D-T} = \frac{FWHM^{source}_{D-T}}{FWHM^{yield}_{D-T}} = 7.50$$

in order to estimate the ion temperatures using $(2a)$ and the sensitivity $(2b)$. The numerical values estimated are

$$FWHM^{yield}_{D-D} = 150 \pm 7\ KeV \qquad FWHM^{yield}_{D-T} = 75 \pm 4\ KeV$$

$$T_i \simeq 1.20 \cdot 10^5\ K$$

in good agreement with the literature [3, 6]

5. Neutron kinematics analysis

A simple analysis of the elastic scattering processes of neutrons has been supported with the help of neutron kinematics in order to reach a better knowledge of energy–loss phenomena occurring during a neutron history along the horizontal port. The spectrum obtained at the exit of the horizontal channel broadens as mentioned and yields on energies far from the narrow–peak distributions are found.

The iron made pin–hole inside the port seems to be the only candidate to collision processes, so elastic $n - Fe$ scatterings has to be taken into account to estimate the afore mentioned energy decreasing. In the laboratory frame, a completely elastic scattering of a non–relativistic neutron can be described as a negative variation of its energy from an initial value E_0 to a final one $E < E_0$ by the equation [8]

$$\frac{dE}{E_0} = \frac{2A}{(1-A)^2} d(\cos\theta) \tag{7}$$

where θ is the lab scattering angle and A is the atomic weight of the target nucleus. The value E after a single collision lies in the interval $\alpha E_0 \le E \le E_0$, being

$$(A-1)^2$$

and the scattering probability takes the form

$$dW = \frac{dE}{E_0(1-\alpha)} \quad . \tag{8}$$

The letargy can then be defined as $u = \log(E_0/E)$ and its value, averaged over the quoted interval, depends only on the nature of the target and not on the dynamics of the incoming neutron. Indeed

$$\overline{u} = \int_{\alpha E_0}^{E_0} \log(E_0/E)\frac{dW}{dE}dE = \log E_0 - < \log E >$$

$$= 1 + \frac{(A-1)^2}{2A}\log\frac{A-1}{A+1} \quad . \tag{9}$$

It is then possible to state that *one* collision decreases the average letargy value from $\log E_0$ to $< \log E >$ and, as a natural generalization, k collisions give rise to the formula

$$< \log E_k >= \log E_0 - k \cdot \overline{u} \quad . \tag{10}$$

With simple algebraic manipulation of (10) it is possible to extract the number of elastic scatterings occurred by a neutron observed at an energy E. Assuming that the mean value E_m related to each bin in the MCNP output histogram represents the final energy, it is possible to estimate the most probable number of elastic processes $n - Fe$ which have removed neutrons from D–D or D–T characteristic peak energies,

$$E_m \cong E_k = \int_{\alpha E_{k-1}}^{E_{k-1}} E\frac{dW}{dE}dE = \frac{1+\alpha}{2}E_{k-1} \quad . \tag{11}$$

Intervals and probabilities can be redefined as

$$[\alpha E_{k-1}, E_{k-1}] \equiv [\frac{2\alpha}{1+\alpha}E_m, \frac{2}{1+\alpha}E_m]$$

$$dW = \frac{1+\alpha}{1-\alpha}\frac{1}{2E_m}dE \quad , \tag{12}$$

while the discrete set of output energies written as

$$< \log E_m >= \int_{2\alpha E_m/(1+\alpha)}^{2E_m/(1+\alpha)} \log E \cdot \frac{dW}{dE}dE$$

$$= \log\frac{2E_m}{1+\alpha} - 1 - \frac{\alpha}{1-\alpha}\log\alpha \quad , \tag{13}$$

and combined with (10) to obtain the mentioned number of collisions k. For our purposes the starting energies E_0 have been chosen as the fusion energies of the D–D and D–T nuclear reactions. Errors can be estimated by means of the canonical variance calculation which suggests that the relative error

$$\frac{\Delta E_m}{E_m} = \frac{1}{\sqrt{3}} \frac{1-\alpha}{1+\alpha} \tag{15}$$

does not depend on the energy but only on the nature of the target by means of α defined at the beginning of the paragraph. In the case of elastic neutron scattering on Fe the calculations give the value

$$\frac{\Delta E_m}{E_m} = 2.06 \cdot 10^{-2} \quad .$$

Results of number of collisions vs. final energy E_m for neutrons with D–D and D–T typical starting energies are shown in Fig.4 .

6. Conclusions

Monte Carlo simulations of neutron fluxes produced in D–D and D–T fusion reactions have been performed and kinematics analysis carried out in order to predict results of plasma diagnostics with neutrons.

Statistical errors resulting from Monte Carlo calculations vary over a narrow range for each bin. Their values are ~ 7 % on energies in the neighbourhood of the fusion peaks, and increase up to ~ 15 % at very low energies and mostly in the central region between D–D and D–T, due to the fact that the number of neutrons dropping from D–T peak to lower values are practically the only ones which contribute [9]. Then the statistics comes out to be less significative and error bars increase consequently.

The pin hole structure has been shown to be very useful in selecting the sight angle and detecting neutron fluxes coming from different sections of the plasma. This provides a kind of spatial resolution of neutron spectrum and a more accurate diagnostics set up.

On the other hand, the pin–hole walls are responsible of the neutron scatterings as suggested by kinematics calculations and the proof can be easily deduced by the yields plot at large detection angles with respect to the ones evaluated at θ_0. Fluxes travelling near the Fe walls are in fact more affected by elastic collision processes and a higher yield on energies well far from the source peaks appear as a direct consequence.

Acknowledgements

The authors wish to thank Dr. Ing. R. Dierckx of J.R.C. – Ispra (Varese) for the helpful discussion on plasma diagnostics and precious suggestions in MCNP optimizations.

References

[1] MCNP - *A general purpose Monte Carlo code for neutron and photon transport* , LA-7396-M Rev Version 2B, Los Alamos Monte Carlo Group, Los Alamos National Laboratory (1982)

[2] M. Pillon, K.A. Verschuur, O.N. Jarvis, J. Källne and M. Martone - *Calibration of neutron yield activation measurements at JET using MCNP and FURNACE neutron transport codes* , JET-P(88)08, February 1988

[3] R. Dierckx - *IGNITOR: particle diagnostics and physics R & D* ,working paper, EURATOM (Ispra), November 1988

[4] K.A. Verschuur - *Parameter study on poloidal response distribution in toroidal geometries* , Proc. 11^{th} SOFT Conference, Oxford (1980) p.197

[5] M.T. Swinhoe and O.N. Jarvis, Rev. Sci. Instr. 56 (1985) 1093

[6] O.N. Jarvis, M.T. Swinhoe and P. Dixon - *Proposed diagnostic systems for JET* - 4^{th} ASTM-Euratom Symposium on Reactor Dosimetry, NBS - Washington, March 22-26, 1982

[7] K.A. Verschuur - *Neutron transport calculations in support of neutron diagnostics at JET* , Netherlands Energy Research Foundation Report, ECN–86–097

[8] P. Batistoni, M. Martone, M. Pillon, M. Rapisarda and J. Argyle *Studies of tritium burnup in JET deuterium plasmas* , Proc. 14^{th} European Conference on Controlled Fusion and Plasma Physics, Madrid vol.3 (1987) p.1228

[9] E. Segré - *Nuclei and Particles* - 2^{nd} edition, W.A. Benjamin Inc., Berkeley (1977)

Figure Captions

Fig. 1 . Scheme of the computer simulated vacuum vessel and horizontal port.

Fig. 2a–e . Neutron yield histograms in the five detection cells obtained from MCNP simulations.

Fig. 3 . Example of the fitting of the peaks D–D and D–T and of the estimation of $FWHM$s. Values are referred to the central cell.

Fig. 4 . Calculated number of collisions occurred by neutrons with D–D and D–T typical fusion energies vs. possible final energies at the end of the horizontal port.

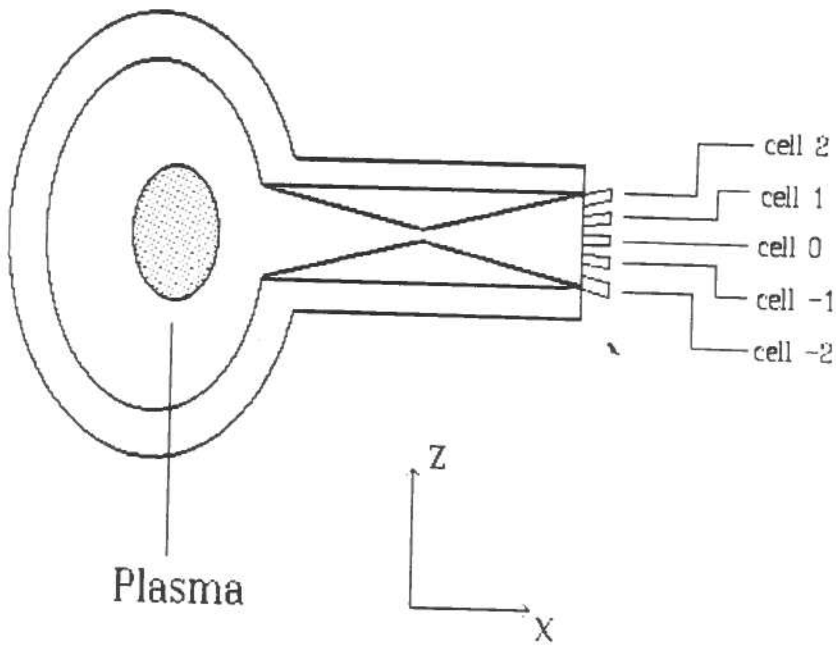
cell 2
cell 1
cell 0
cell -1
cell -2
Z
Plasma
X

FIG. 1

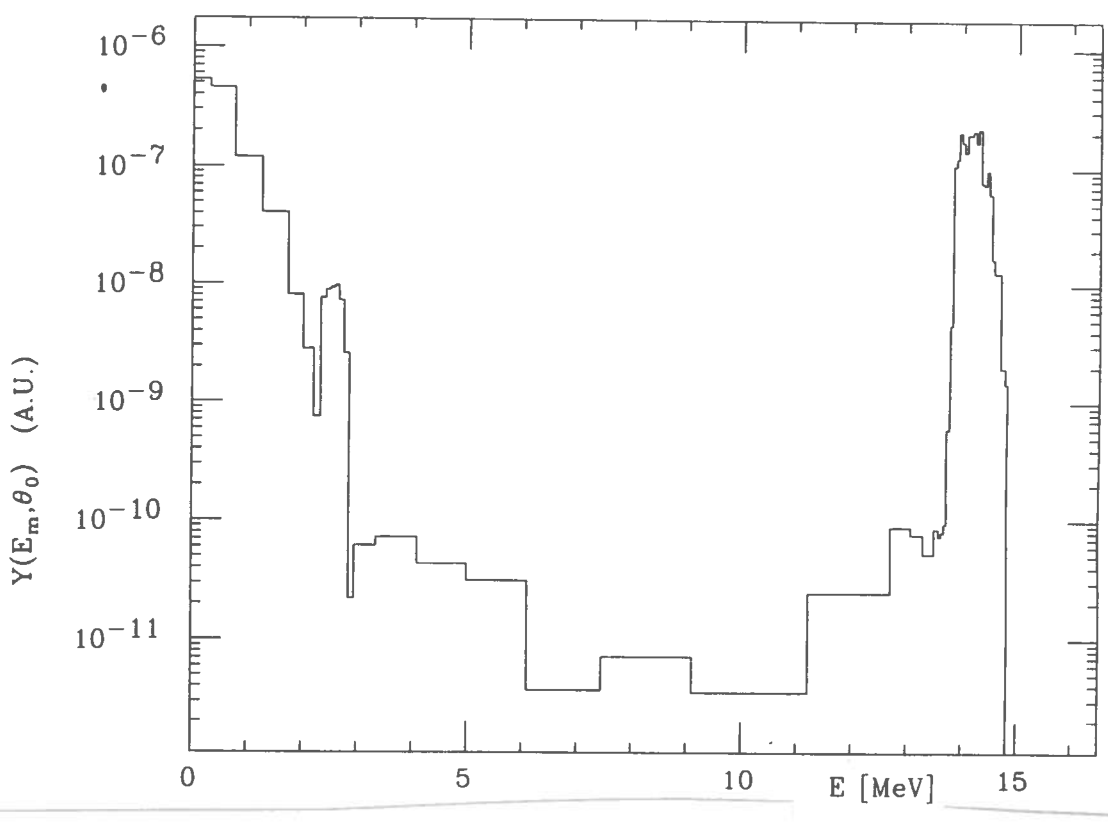
10^{-6}
10^{-7}
10^{-8}
10^{-9}
10^{-10}
10^{-11}
$Y(E_m,\theta_0)$ (A.U.)
0
5
10
15
E [MeV]

FIG. 2a

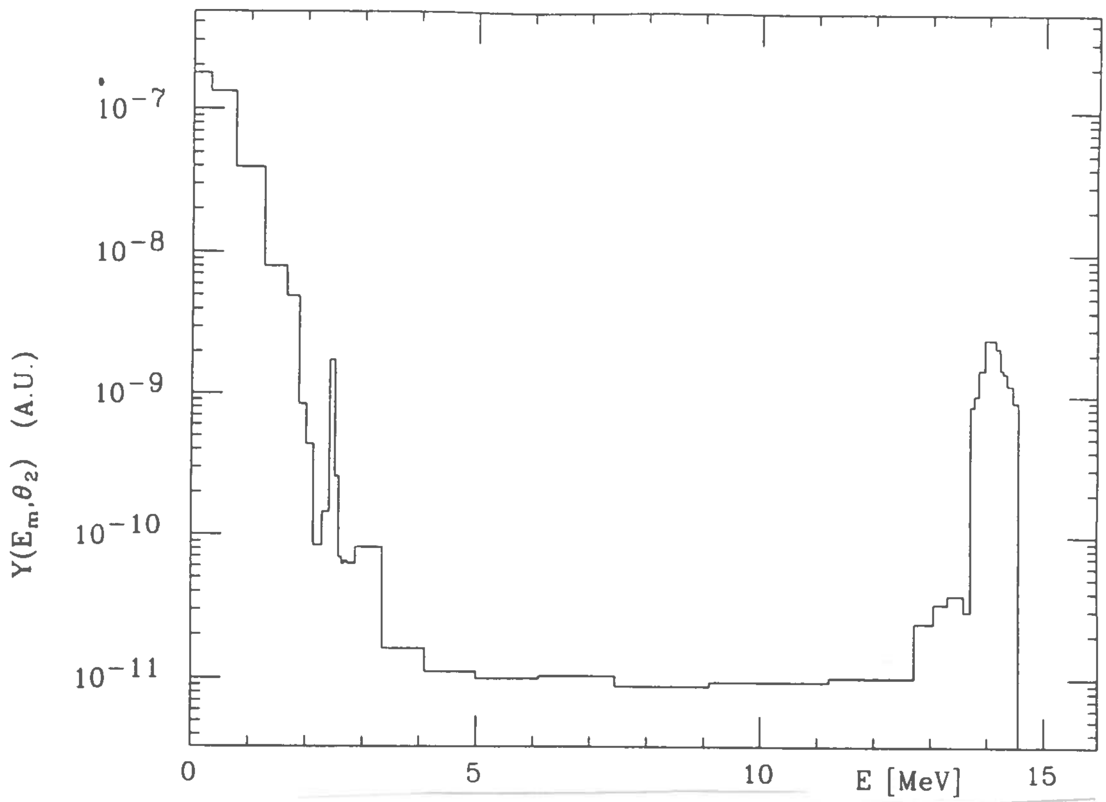
10^{-7}
10^{-8}
10^{-9}
10^{-10}
10^{-11}
$Y(E_m,\theta_2)$ (A.U.)
0
5
10
E [MeV]
15

FIG. 2b

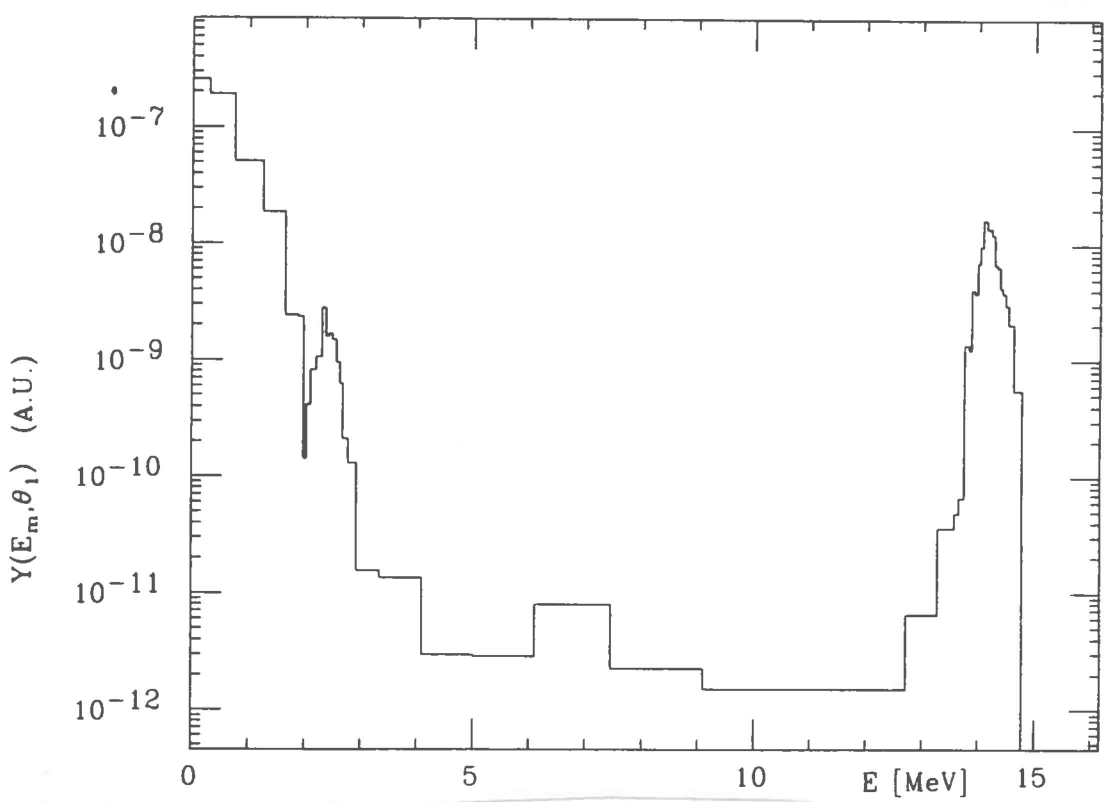
10^{-7}
10^{-8}
10^{-9}
10^{-10}
10^{-11}
10^{-12}
$Y(E_m,\theta_1)$ (A.U.)
0
5
10
E [MeV]
15

FIG. 2c

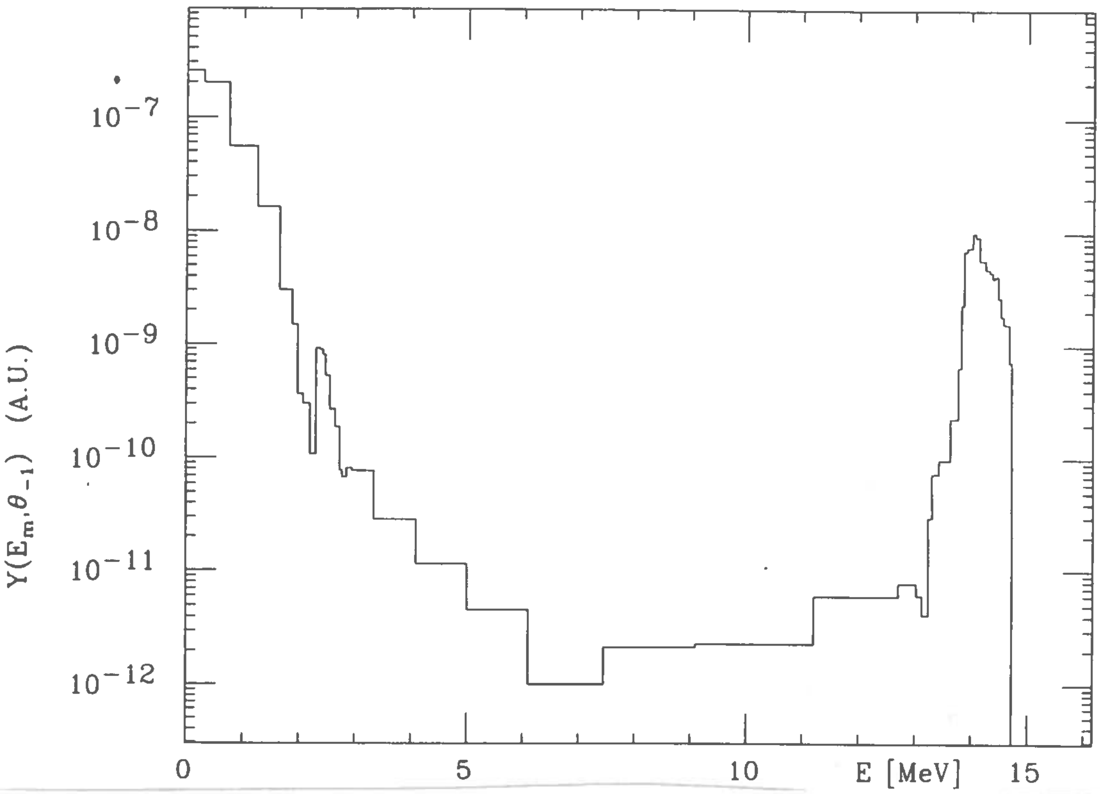
10^{-7}
10^{-8}
10^{-9}
10^{-10}
10^{-11}
10^{-12}
$Y(E_m,\theta_{-1})$ (A.U.)
0
5
10
15
E [MeV]

FIG. 2d

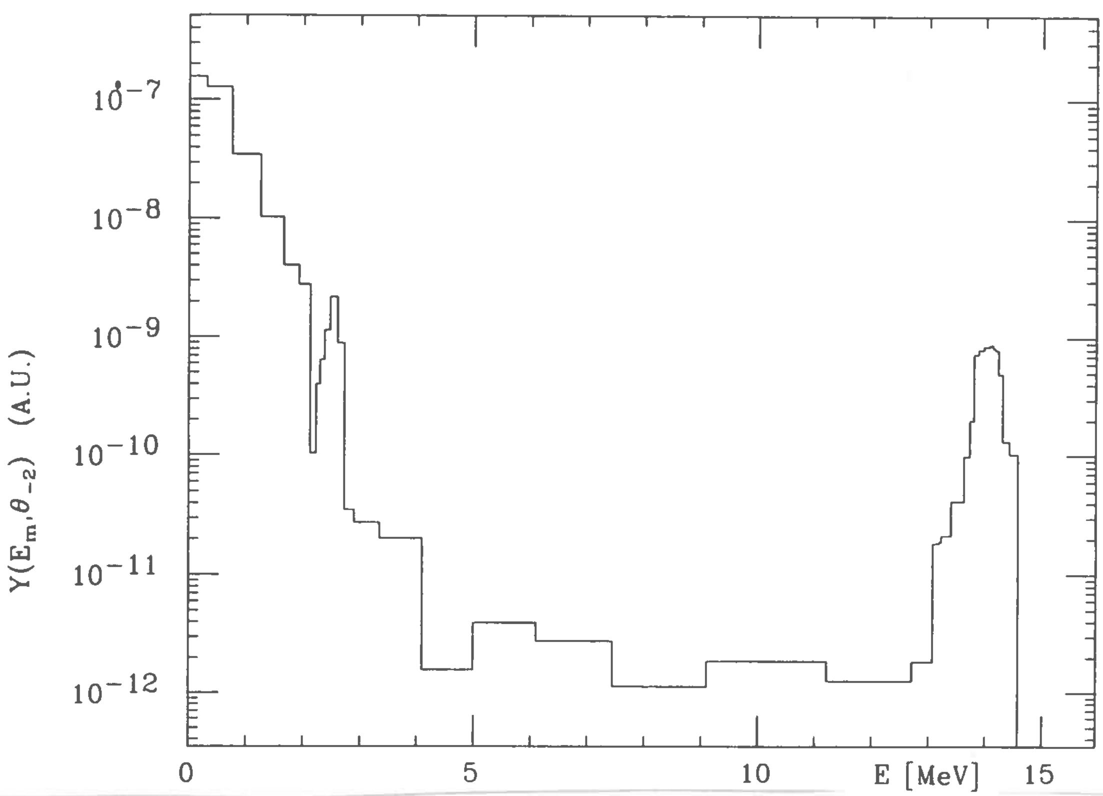
10^{-7}
10^{-8}
10^{-9}
10^{-10}
10^{-11}
10^{-12}
$Y(E_m,\theta_{-2})$ (A.U.)
0
5
10
15
E [MeV]

FIG. 2e

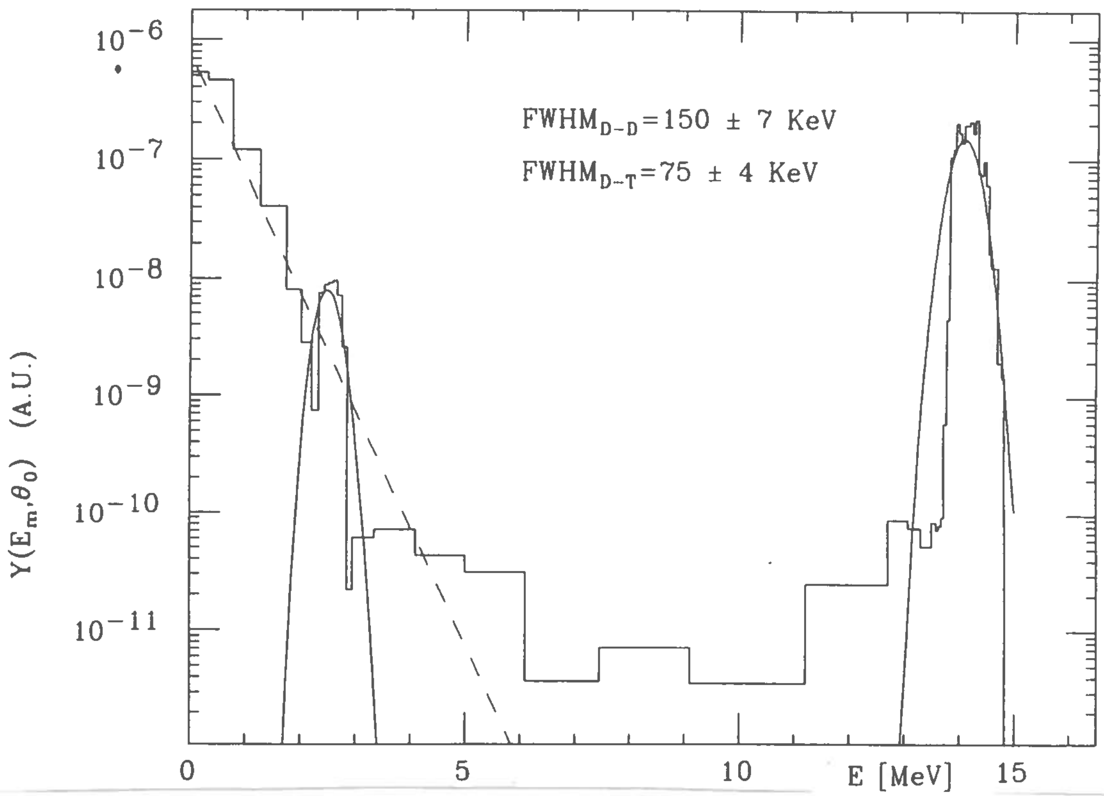

10^{-6}
10^{-7}
10^{-8}
10^{-9}
10^{-10}
10^{-11}
$Y(E_m,\theta_0)$ (A.U.)
$FWHM_{D-D}=150 \pm 7$ KeV
$FWHM_{D-T}=75 \pm 4$ KeV
0
5
10
15
E [MeV]

FIG. 3

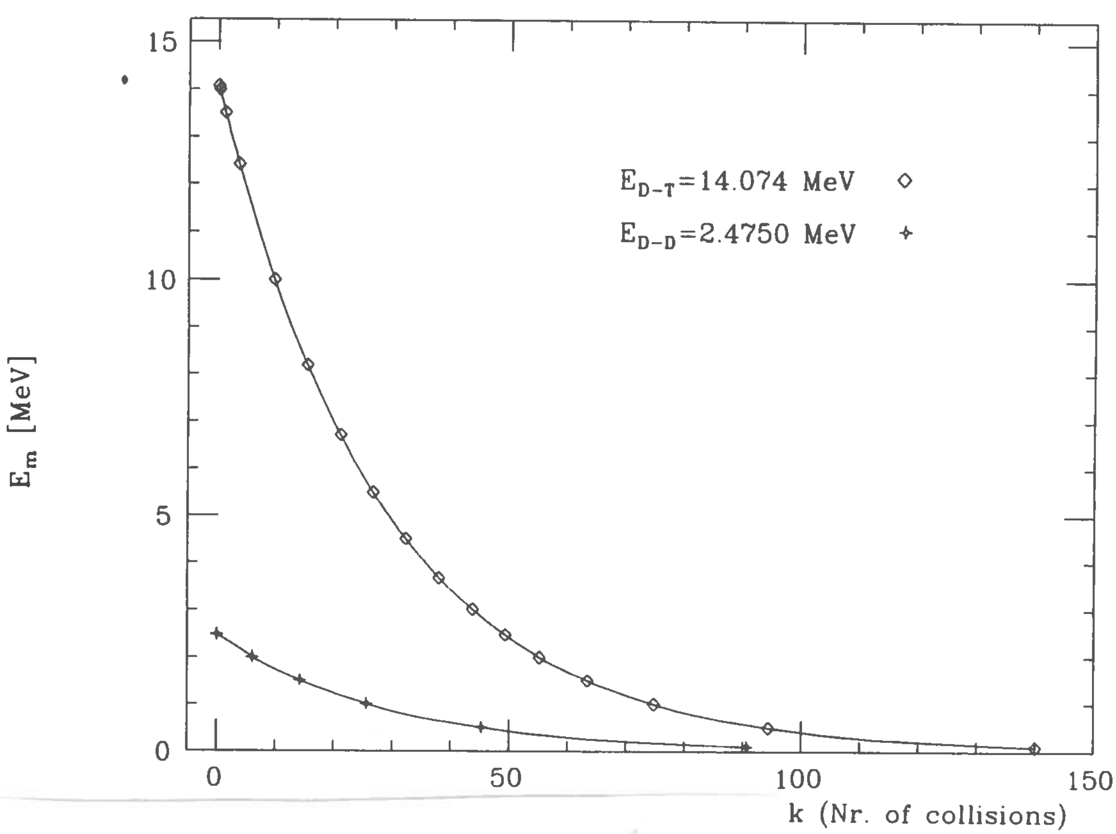

15
10
5
0
E_m [MeV]
$E_{D-T}=14.074$ MeV
$E_{D-D}=2.4750$ MeV
0
50
100
150
k (Nr. of collisions)

FIG. 4